

Sensitivity of Tsunami Uplift Impact to Wharf Properties

Cheng Chen¹, Napayalage A. K. Nandasena^{2*} and
Bruce W. Melville³

¹College of Civil Engineering
Fuzhou University
Fuzhou 350108, P. R. China

²Department of Civil and Environmental Engineering
United Arab Emirates University
Al Ain 15258, United Arab Emirates
*n.nandasena@uaeu.ac.ae

³Department of Civil and Environmental Engineering
The University of Auckland
Auckland 1142, New Zealand

Date received: May 15, 2021

Revision accepted: November 1, 2021

Abstract

To elucidate the tsunami-wharf interaction (e.g., flow field and pressure distribution), a numerical study was carried out to simulate a wharf subjected to a tsunami bore. A dam-break-like tsunami bore was simulated by modeling a gate-reservoir system. Five sections (reservoir, wet-bed, transitional, dry-bed and wharf model sections) were established to investigate the generation, propagation, stabilization of dam-break-like tsunami bore and impact on the model. The bore characteristics on the wet and dry bed were extracted; tsunami pressures and the flow field around the wharf model were presented. Validation against a laboratory study showed that the computed pressure on the wharf was more accurate with a mild wharf slope than a steep wharf slope (less than 20% errors for 20 to 50°). The flow motion in the numerical flume consisted of the generation (0.5 s), stabilization (1.0 s), propagation (2.5 s) and impact stages (2.5 s). The flow velocity fields for the tsunami bore partly depended on the bed conditions due to momentum exchange between the tsunami bore and still water. The tsunami bore impacts on the wharf consist of four stages (front-climbing, front-hitting, water accumulation and quasi-steady), with the highest uplift pressures (5.5-6.7 kPa) occurring in the front-hitting stage when the bore first reached the wharf deck. The average tsunami uplift pressures exerting on the deck decreased with increasing deck length, deck-slope gap and slope surface roughness implicating three tsunami energy dissipation factors in the wharf design.

Keywords: numerical model, pressure contour, tsunami bore, velocity field, wharf

1. Introduction

Tsunamis triggered by earthquakes have occurred frequently in the recent past, and consequently, many researchers have focused on tsunami-structure interaction. Major tsunamis such as the 2004 Indian Ocean Tsunami, the 2010 Chile Tsunami and the 2011 Tohoku Tsunami have resulted in devastating damage to coastal structures. A tsunami is a series of waves in a water body caused by the sudden displacement of a large volume of water. In the ocean, the propagation speed of the tsunami wave can be about 190-210 m/s (Chao and Liu, 2014). When the tsunami approaches the coast, wave shoaling increases the amplitude of the tsunami wave, which grows enormously in amplitude as it advances towards the shoreline. From video recordings of the 2004 Indian Ocean Tsunami, the tsunami propagating onshore appears similar to a fast-moving hydraulic bore and continues as an overland flow impacting infrastructures (Nouri *et al.*, 2010). Besides, open bays and coastlines adjacent to very deep water may shape a tsunami bore into a step-like wave with a steep-breaking front.

Due to close agreement between the analytical solution and tsunami field data (Chanson, 2006), a dam-break hydraulic bore has been widely used in laboratory experiments to simulate a tsunami bore (Nandasena and Tanaka, 2013; Rahman *et al.*, 2014; Wei *et al.*, 2016). Lauber and Hager (1998) investigated the dam-break flow using physical modeling in a smooth, rectangular channel. They realized that the effect of both the bottom slope and viscosity on the positive and negative wavefronts is significant. For a dam-break flow over a rough slope, Deng *et al.* (2016) presented an analytical solution based on the method of characteristics. Liu *et al.* (2017) verified the basic hydrodynamic features of the dam-break flow at the gate location. They showed that the temporal variation of the water surface elevation can be divided into a sharp decreasing stage, a relatively steady stage, and a gradually decreasing stage. Based on a two-liquid volume of fluid (VOF) model, Ye and Zhao (2017) carried out a numerical study to investigate dam-break flow on a wet bed. The effects of gate thickness, gate removal velocity and depth of ambient water were illustrated in their study.

Some experimental studies have been undertaken to simulate coastal structures subjected to a dam-break-like tsunami bore. Kihara *et al.* (2015) investigated tsunami impacts on a wall and found that in the initial reflection phase, high pressure was exerted on the wall due to the collapse of the water column, while in the quasi-steady-state phase, the pressures were almost equal

to the hydrostatic pressure upstream of the wall. Ko and Ye (2018)'s experimental results suggest that the flow near the splash-up tip behaves like a solid-body projectile. Shafiei *et al.* (2016, 2018) studied the tsunami impacts on standing structures, measuring the three-dimensional pressure distribution around a cylinder. They found that the values of the hydrodynamic forces after bore impact demonstrated a drag coefficient equal to 0.65. The corresponding drag coefficient for a square prism was found to vary with the orientation concerning the tsunami flow direction. Chen *et al.* (2018) investigated the tsunami loads on a bridge and found that the load depends not only on the stage of the tsunami flow but also on the structural style. For tsunami impacts on a wharf, the total uplift load increases with increasing bore height or decreasing deck height, and it is also affected by the slope angle under the wharf deck (Chen *et al.*, 2016).

Numerical studies on dam-break-like tsunami flow have also been performed. The dam-break flow numerical models can be classified into two major approaches – mesh-based methods and mesh-free methods. Smoothed particle hydrodynamics (SPH) is one of the mesh-free methods. With an SPH model, Crespo *et al.* (2008) analyzed dam break evolution over both dry and wet beds. To calculate the water wave pressure on impact, Zheng *et al.* (2014) introduced a truly incompressible SPH (ISPH) technique using a pressure Poisson equation. Wei *et al.* (2016) implemented a weakly compressible SPH method to simulate nearshore tsunami processes.

The VOF method is one of the mesh-based approaches. With the VOF method, Biscarini *et al.* (2010) investigated the dam-break flow based on Reynolds-Averaged Navier-Stokes equations. Liu *et al.* (2017) examined the evolution of dam-break flow over complicated terrain using 3D numerical simulation. The dam-break flow over uneven beds was studied by Marsooli and Wu (2014) using a VOF-based model. Numerical simulation of the propagation of a tsunami bore over a hump of different slopes was performed by Cheng (2017) based on the VOF method.

However, the tsunami bore impact on a wharf has not yet been numerically investigated. Some detailed analyses are beyond the resolution of small-scale experimental studies and have, therefore, not been carried out. In this study, the numerical results for the tsunami pressure on a wharf were validated against the previous experimental data (Chen *et al.*, 2016). The interaction of tsunami with the wharf for the various conditions has then been discussed. The innovative contribution of this paper is the elucidation of complicated pressure

distribution and the flow field around the wharf due to tsunami interaction, which could not easily be obtained by physical experiment. On the other hand, it helps one to better understand the real phenomenon in the nature.

2. Methodology

2.1 Laboratory Experiment

The data for validating the numerical model given in section 2.2 was taken from the experiments conducted by Chen *et al.* (2016). These laboratory experiments were conducted in the tsunami wave flume at the University of Auckland, New Zealand. A reservoir and the flume were separated by a steel sluice gate. When the sluice gate was lifted, the water rushed from the reservoir into the tsunami wave flume that generated a dam-break-like tsunami bore.

To represent a typical wharf model, a deck-slope structure was installed on the dry bed at the end of the flume. The deck-slope model consists of a horizontal deck, an adjustable slope and six steel piles along the transverse direction. The wharf deck heights were selected as 0.20, 0.25 and 0.30 m above the dry bed. The slope angles (under the horizontal deck) were selected as 20, 25, 30, 35, 40, 45, 50 and 90°. The wharf model was 1.2 m long in the direction transverse to flow orientation. The deck and slope were made of 15-mm thick acrylic sheet. The width of the deck was 0.22 m representing a real wharf deck of 11 m width. The tsunami bore heights in the test were 0.15, 0.17, 0.19, 0.21, 0.22, 0.25 and 0.28 m. The bore Froude number was estimated 1.6 for most of the cases. Eight pressure sensors were used to capture the tsunami pressures on the soffit of the deck. Therefore, time-histories of pressure on the soffit of the deck were measured; the effects of bore height, deck height and slope angle on uplift pressures were experimentally studied.

2.2 Governing Equations

In this study, a computational fluid dynamics (CFD) code FLOW-3D (Flow Science, Inc., 2012) was used to numerically investigate the impact of a dam-break-like tsunami bore on a wharf. FLOW-3D implements the finite volume method to solve the Reynolds-averaged Navier-Stokes equations, with a VOF method to track the free surface. The seawater was assumed to be an incompressible viscous fluid, and the continuity equation and momentum

conservation equation were applied to describe the fluid motion. The continuity equation is presented as Equation 1.

$$V_f \frac{\partial \rho}{\partial t} + \frac{\partial}{\partial x} (\rho u A_x) + \frac{\partial}{\partial y} (\rho v A_y) + \frac{\partial}{\partial z} (\rho w A_z) = 0 \quad (1)$$

where V_f is the fraction of open volume to flow; ρ is the water density; (u, v, w) are the components of velocity in the three directions (x, y, z) ; (A_x, A_y, A_z) are the fractions of open levels in the three directions (x, y, z) , respectively.

Momentum equations with velocity components of (u, v, w) in three directions (i.e., Navier-Stokes equations) are presented as Equations 2, 3 and 4.

$$\frac{\partial u}{\partial t} + \frac{1}{V_f} \left\{ u A_x \frac{\partial u}{\partial x} + v A_y \frac{\partial u}{\partial y} + w A_z \frac{\partial u}{\partial z} \right\} = -\frac{1}{\rho} \frac{\partial p}{\partial x} + G_x + f_x \quad (2)$$

$$\frac{\partial v}{\partial t} + \frac{1}{V_f} \left\{ u A_x \frac{\partial v}{\partial x} + v A_y \frac{\partial v}{\partial y} + w A_z \frac{\partial v}{\partial z} \right\} = -\frac{1}{\rho} \frac{\partial p}{\partial y} + G_y + f_y \quad (3)$$

$$\frac{\partial w}{\partial t} + \frac{1}{V_f} \left\{ u A_x \frac{\partial w}{\partial x} + v A_y \frac{\partial w}{\partial y} + w A_z \frac{\partial w}{\partial z} \right\} = -\frac{1}{\rho} \frac{\partial p}{\partial z} + G_z + f_z \quad (4)$$

where p indicates pressure; G_x, G_y, G_z are mass accelerations in three directions (x, y, z) ; f_x, f_y, f_z are viscosity accelerations in three directions (x, y, z) .

2.3 Numerical Flume Setup

A computational area was established to simulate the numerical flume model. The area was 26 m long (in the x-direction), 0.1 m wide (in the y-direction) and 0.85 m high (in the z-direction) consisting of 2,210,000 computational cells (0.01 m grid size). As shown in Figure 1, there were five different sections in the x-direction (i.e., reservoir, wet-bed, transitional, dry-bed and wharf model sections). A sluice gate with a thickness of 0.1 m was set in between the reservoir and wet-bed sections. The ramp section modeled a ramp between the dry- and wet-bed sections allowing a mild transition in the bed elevation. In the wharf model section, a deck-slope model was installed on the dry bed. The configuration of the wharf model was alterable to the experimental requirement accordingly (section 2.4). The bore Froude number in this tsunami wave flume was suitable for tsunami simulation according to tsunami bore velocity of the building code of the City and County of Honolulu (CCH) (2000) and Federal Emergency Management Agency (FEMA) (2012).

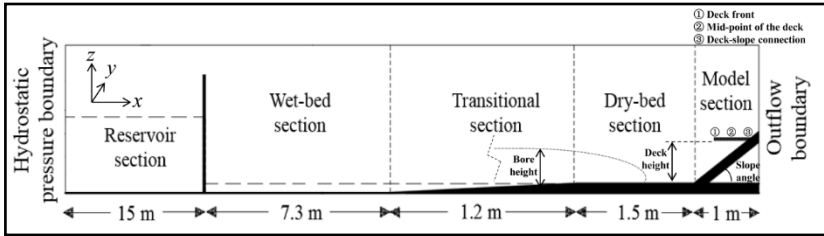


Figure 1. Cross section of the tsunami wave flume

2.4 Setup of Wharf Configuration Variations Related to Tsunami Pressure

The tsunami loads exerted on the deck are affected not only by the bore characteristics but also by the wharf configurations such as deck height, slope angle, deck length, deck-slope gap, slope's surface roughness, etc. However, the physical experiments did not investigate the effects of the deck length, deck-slope gap and slope surface roughness on the tsunami loads. Therefore, these wharf configuration variations were implemented in this numerical study (Figure 2).

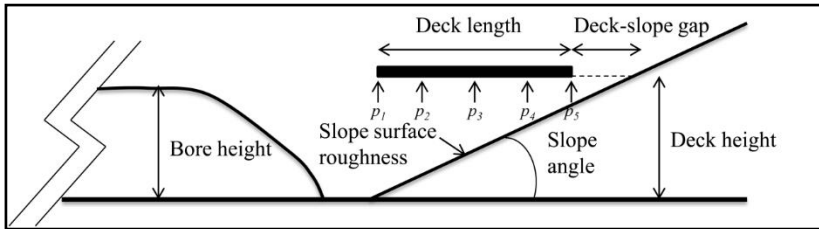


Figure 2. Variable parameters of the wharf model for sensitivity analysis

To investigate the deck length effect, the following parameters were kept constant: the deck height was 0.25 m, the tsunami bore height was 0.28 m, the wharf slope was 30° and there was no deck-slope gap. The deck length varied between 0.05 m (0.2 times the deck height) and 2 m (8 times the deck height).

In determining the deck-slope gap effect, the following parameters were kept constant: the deck length, deck height, and tsunami bore height were 0.22, 0.25 and 0.28 m, respectively; the wharf slope was 30° . The deck-slope gap varied between “no gap” and a gap of 0.110 m (50% of the deck length).

In the numerical model, the tsunami pressures on the deck were also affected by the slope's surface roughness. In a real situation, the slope roughness can vary with the choice of revetment materials. To examine the effect of this

roughness, the following parameters were kept constant: the deck length, deck height and tsunami bore height were 0.22, 0.25 and 0.28 m, respectively; the wharf slope was 30°; and there was no deck-slope gap. Simulated values of slope surface roughness k_s were 0.01 m (4% of the bore height), 0.02 m (7% of the bore height) and 0.05 m (18% of the bore height), as well as zero roughness. k_s can be related to Manning's n by $k_s = (n/0.0389)^6$, where n has units of $m^{1/6}$.

2.5 Initial and Boundary Conditions

In the computational area, different boundary conditions were selected and applied. In the z -direction, the lower boundary was set as an impermeable wall, and the upper boundary was zero outflows. In the y -direction, both boundaries were “symmetrical” (i.e., no inflow or outflow and zero gradients in the y -direction), which means that any effect from the side walls was ignored. In the x -direction, the upstream boundary was a constant hydrostatic pressure boundary (0.4, 0.5, or 0.6 m) corresponding to the reservoir water level; and the downstream boundary was an outflow boundary. The surface roughness was assumed to be zero for validating experimental results.

At the start of the simulation, the reservoir level was set to the water level of one of the flume experiments (i.e., 0.4, 0.5, or 0.6 m). Also, water with a surface elevation of 0.05 m was assumed in the wet bed section and transitional section. The sluice gate is closed at the start of the simulation but is then opened immediately as shown in Figure 3 for three different gate openings (0.2, 0.3 and 0.4 m) to create the dam-break-like tsunami bore.

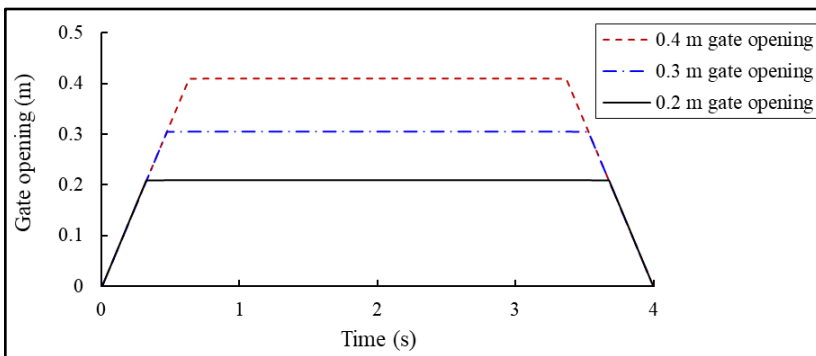


Figure 3. Time-history of the gate opening for generating different tsunami bore heights

The bore shape from this sluice gate was similar to the tsunami bore shape, which washed ashore and then hit the structures (CCH, 2000; FEMA, 2012). The total simulation time was 7 s in every case.

3. Results and Discussion

3.1 Time-history of Pressure

The numerical simulation results of the time histories of pressure exerted on the mid-point of the deck were compared with those from the previous physical experiment (Chen *et al.*, 2016). The following experimental setups are shown in this paper: (1) slope angles of 20, 30, 40, 50 and 90° (vertical wall); (2) deck height above the dry bed of 0.25 m; (3) tsunami bore heights (Figure 1) of 0.17 and 0.28 m.

Figure 4 shows the validation results. For small slope angles, the simulation results of this numerical model agreed reasonably well with the physical experimental results, especially for peak pressure and quasi-steady pressure. However, the accuracy of the simulation gradually reduced with increasing slope. Simulating the pressures with the 90° slope was particularly imprecise. To be more specific, with increasing slope angle, the simulated pressures oscillated randomly to a greater degree. This may be due to the high-speed tsunami flow breaking with the air-entrained through the interface, and the splash increased with an increasing slope angle. For the 90° slope (i.e., a vertical wall), the tsunami flow was reflected by the wall, and the reflected flow encountered the upcoming flow with large splashes. It can be confirmed that this numerical model is suitable for the cases of small wharf slope angles rather than large wharf slope angles based on the results.

3.2 Tsunami Flow in the Flume

When the sluice gate opened, the water in the reservoir rushed into the flume and transformed into a tsunami bore. Figure 5 shows the simulation results of the propagation of the tsunami bore in the flume. The reservoir section on the left of the sluice gate is not shown; thus, the left boundary of Figure 5 is the sluice gate, and on the right is the wharf model. The initial time ($t = 0.0$ s) denotes the start of the sluice gate opening. The flow motion in the flume consisted of four stages.

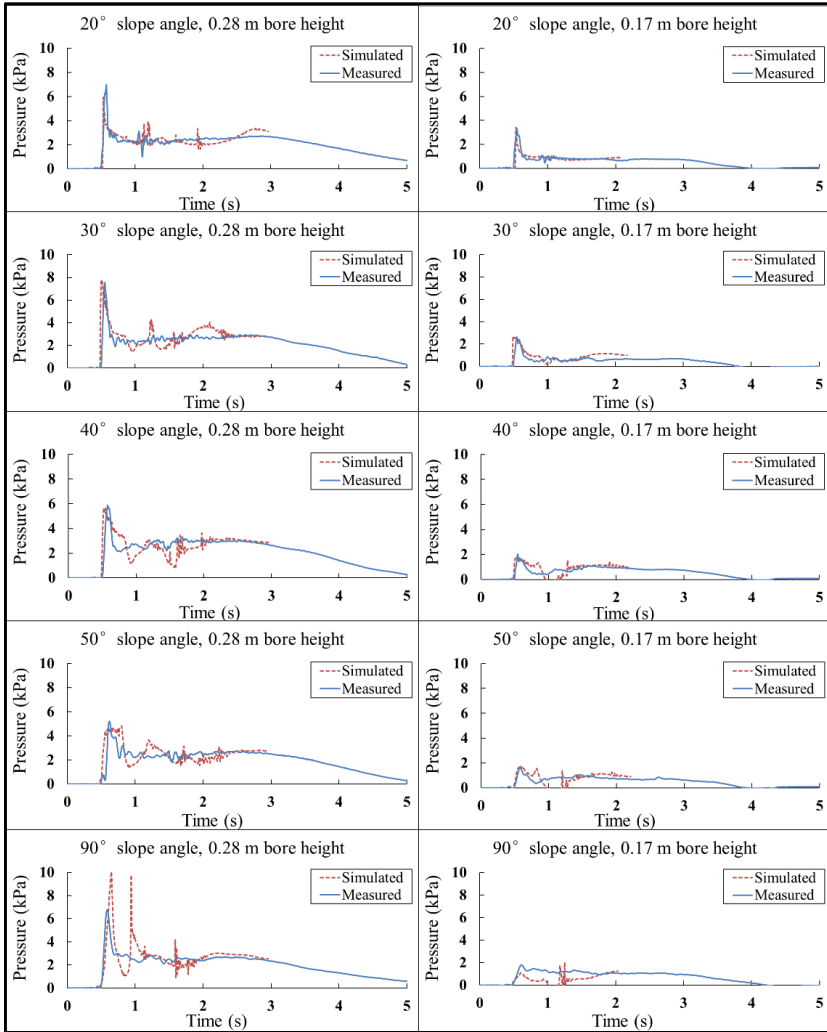


Figure 4. Comparison between the simulated and measured pressures on the mid-point of wharf deck with 0.25 m deck height

The first stage was the generation stage ($t = 0.0-0.5$ s). In this stage, the sluice gate was rapidly lifted, and the water was released from the reservoir to the flume. The high-speed flow is called the dam-break flow; the bore front shape was unstable in this stage.

The second stage was the stabilization stage ($t = 0.5-1.5$ s). In this stage, the sluice gate was fully opened, and the water kept rushing from the reservoir to

the flume. The tsunami bore front collapsed to a stable form and interacted with still water in the wet-bed section.

The third stage was the propagation stage ($t = 1.5\text{-}4.0$ s). In this stage, the tsunami bore was stabilized. It traveled on the wet bed ($t = 2.5$ s), traveled on the ramp ($t = 3.0$ s), and then traveled on the dry bed ($t = 3.5$ s). At $t = 4.0$ s, the tsunami bore front reached the toe of the slope. Meantime, the sluice gate was lowering during $t = 3.5\text{-}4.0$ s, and it was closed at $t = 4.0$ s.

The fourth stage was the impact stage ($t = 4.5\text{-}7.0$ s). At this stage, the tsunami bore was impacting the wharf model including the bore front climbing and hitting the deck, and water accumulating in front of the wharf, running up to the maximum.



Figure 5. Temporal and spatial variation of the tsunami bore in the numerical flume

3.3 Flow Velocity Field

The flow velocity field of the tsunami bore varied with bed conditions, such as whether the bed is initially wet or dry, due to the momentum exchange between the tsunami bore and still water. Simulated flow velocity fields during the tsunami bore propagation were extracted from the numerical results and are shown in Figure 6. Figure 6a shows the velocity field in the wet-bed

section. The toe of the bore advanced over still water followed by a gradual transition to a normal velocity profile (i.e., a logarithmic vertical profile in the horizontal velocity, or nearly so). Figure 6b exhibits the velocity field in the transitional section. Here, the toe of the bore advanced over a thinner layer of still water than in the wet-bed section; a similar transition to a logarithmic velocity distribution occurred. Figure 6c projects the velocity field in the dry-bed section. In this simulation, the dry bed offered little flow resistance compared with the wet bed. This resulted in a flatter front to the bore with a relatively constant vertical profile. This result is consistent with the findings of Dressler (1952) and Kihara *et al.* (2015) highlighting that the bore velocity is almost the same as the fluid velocity in the bore.

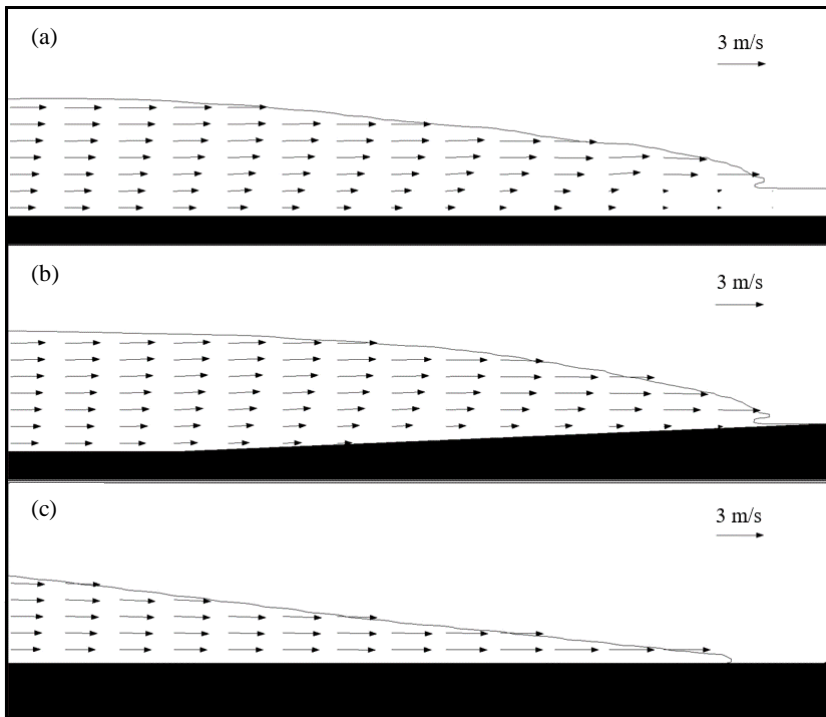


Figure 6. The flow field of the bore front over different bed conditions: wet-bed (a), transitional (b) and dry-bed (c) sections

3.4 Tsunami Bore Impacts on the Wharf

The simulated velocity field and pressure contours of the tsunami bore impacting the wharf model are shown in Figure 7. The impact comprised four stages.

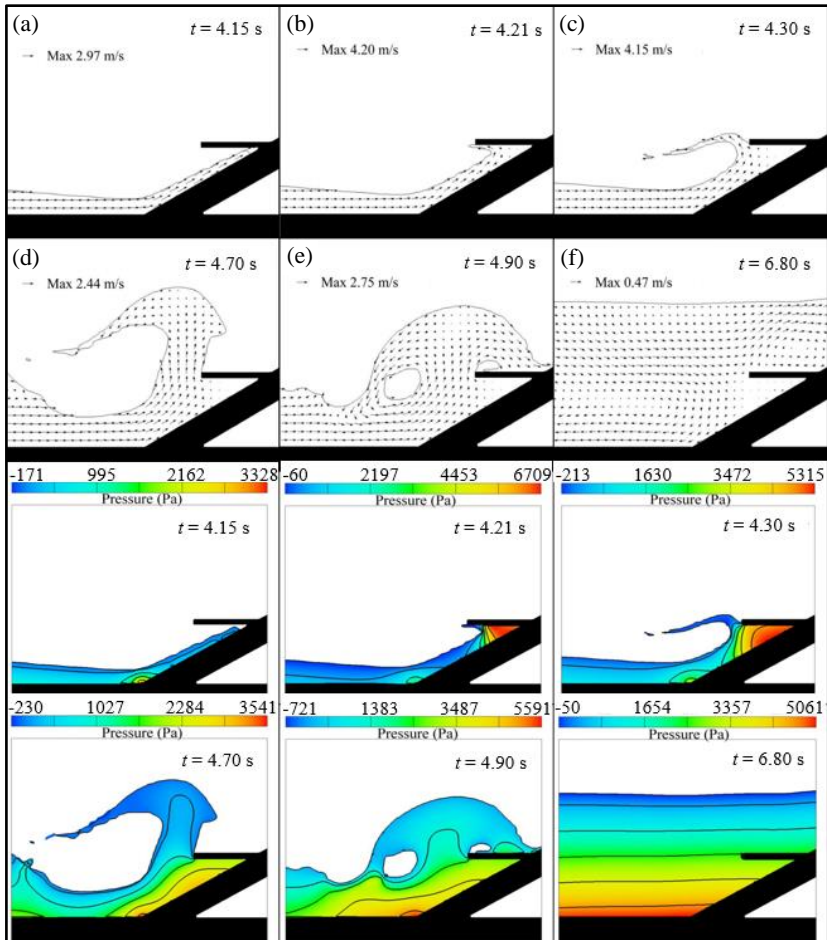


Figure 7. The flow field and pressure distribution around the wharf model in different stages: front-climbing (a), front-hitting (b-d), water accumulation (d-e) and quasi-steady (e-f) stages

In the first stage (Figure 7a) (front-climbing stage [$t = 4.15$]), the toe of the bore front climbs the slope at high speed (about 3 m/s) with the maximum pressure (over 2.7 kPa) occurring at the foot of the slope.

The second stage (Figures 7b-7d) was the front-hitting stage [$t = 4.21-4.70$ s]), wherein the bore front hit the soffit of the deck and splashed back as a jet with a speed up to 4.3 m/s due to the energy concentration under the deck. The maximum pressure (5.5-6.7 kPa) occurred in the area near the deck-slope junction. The high pressures indicated that the wharf deck was most vulnerable to the tsunami bore at this stage.

In the third stage (Figure 7d-7e) (water accumulation stage [$t = 4.70-4.90$ s]), a jet directed vertically upwards split into two parts as it began to fall under gravity ($t = 4.70$). One part of the jet fell onto the surface of the deck, and the other fell in front of the deck back into the main flow. Water accumulated in front of the wharf model; the water level gradually rose with significant oscillations. In this stage, the maximum pressure (3.5-5.6 kPa) took place near the foot of the slope. The pressure exerted on the deck in this stage was between 1.6 and 3.7 kPa.

In the fourth stage (Figure 7e-7f) (quasi-steady stage [$t = 4.90-6.80$ s]), the water level in front of the wharf reached its maximum, and the flow became quasi-steady. The maximum velocity decreased to 0.5 m/s, and velocities under the deck were very low. The pressure contour distribution was close to hydrostatic pressure, and the pressure exerted on the deck (3.3-4.2 kPa) was mainly due to hydrostatic pressure.

3.5 Deck Length Effect on Tsunami Pressure

Different deck lengths in a unit width entrapped different volumes of tsunami bore front. Therefore, the total force on the deck may result in sliding or capsizing of the wharf over a short time. Figure 8 shows the effect of deck length on the average pressure and total force. The average pressure P at any moment is the average value of the pressure exerted on the stream-wise centerline of the deck soffit (i.e., $P = (P1+2*P2+2*P3+2*P4+P5)/8$) (Figure 2), and the average pressure plotted in Figure 8 was the time-average value of P calculated over the front-hitting stage and water accumulation stage. The total force per unit width is the average pressure (P) multiplied by the full deck length. As the figure shows, when deck length was 0.25-1.00 times deck height (i.e., the deck length was not longer than the deck height), the tsunami pressure on the deck was about 2.7 kPa. When the deck length increased by 1-8 times deck height (the deck length was longer than the deck height), the tsunami pressure decreased linearly (from about 2.7 to 1.9 kPa) with increasing deck length. However, the total uplift force increased with increasing deck length because the impact area increased with increasing deck length. Deck lengths of 0.05 and 2.00 m resulted in average tsunami forces on a unit width of the deck of 0.1 and 3.8 kN, respectively.

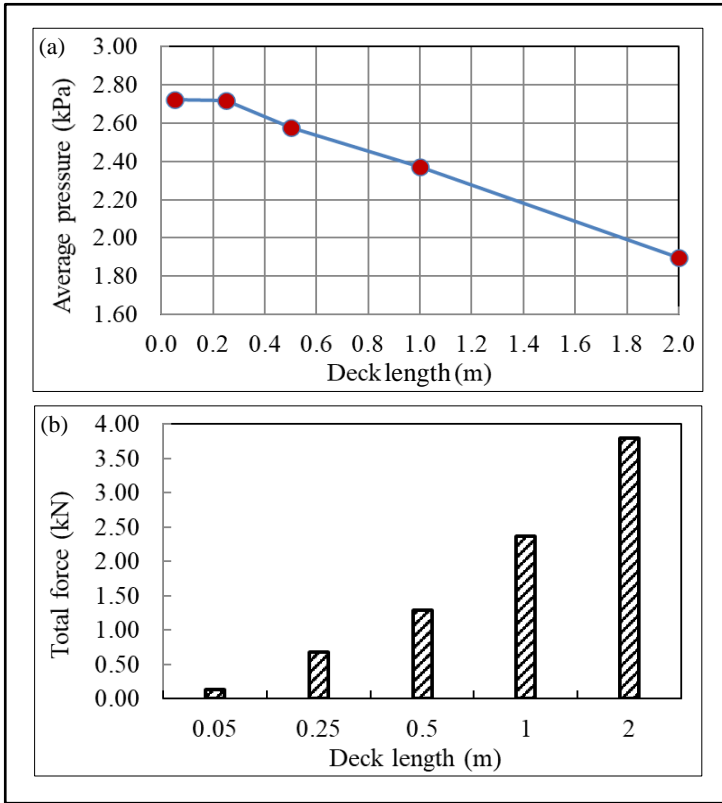


Figure 8. Sensitivity of the tsunami pressure and force to the wharf deck length

3.6 Deck-Slope Gap Effect on Tsunami Pressure

For a pier with the approach trestle, there was a gap between the front platform and the shoreline. During a front-hitting stage in a tsunami event, the deck-slope gap will release the loads from the tsunami bore front, thus mitigate damages. Figure 9a shows the deck-slope gap effect on the average pressure (p) exerted on the deck. These results show that, as the gap increased from 0.000 to 0.110 m, the tsunami pressure decreased from 2.8 to 2.2 kPa. Figure 9b exhibits the reduction factor of the deck-slope gap. The reduction factor is the ratio of the average pressure in each case to the average pressure with no gap. The reduction factor decreased from 1 to 0.81 with the gap increasing from 0 to 50% of the deck length.

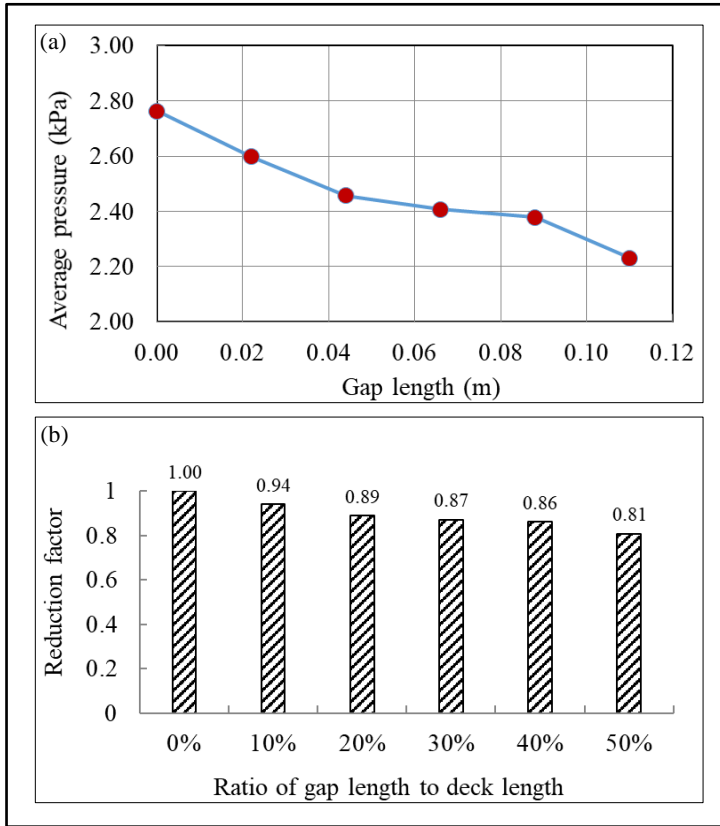


Figure 9. Sensitivity of the tsunami pressure to the wharf deck gap

3.7 Slope Surface Roughness Effect on Tsunami Pressure

In a real situation, revetment materials mounted on the slope contributes to different slope roughness, which reduces the energy of the storm wave and tsunami, especially in the front-hitting stage. Figure 10a projects the effect of the slope surface roughness on the average pressure (p) exerted on the deck. These results showed that the tsunami pressure decreased from 2.8 to 2.5 kPa with surface roughness increasing from nil (smooth slope) to 0.05 m (i.e., a rough slope mitigates the tsunami pressures). Figure 10b displays the reduction factor of the slope surface roughness. The reduction factor is the ratio of the pressure for each case to the pressure for no surface roughness. The reduction factor decreased from 1 to 0.90 with the surface roughness increasing from 0 to 18% of the bore height.

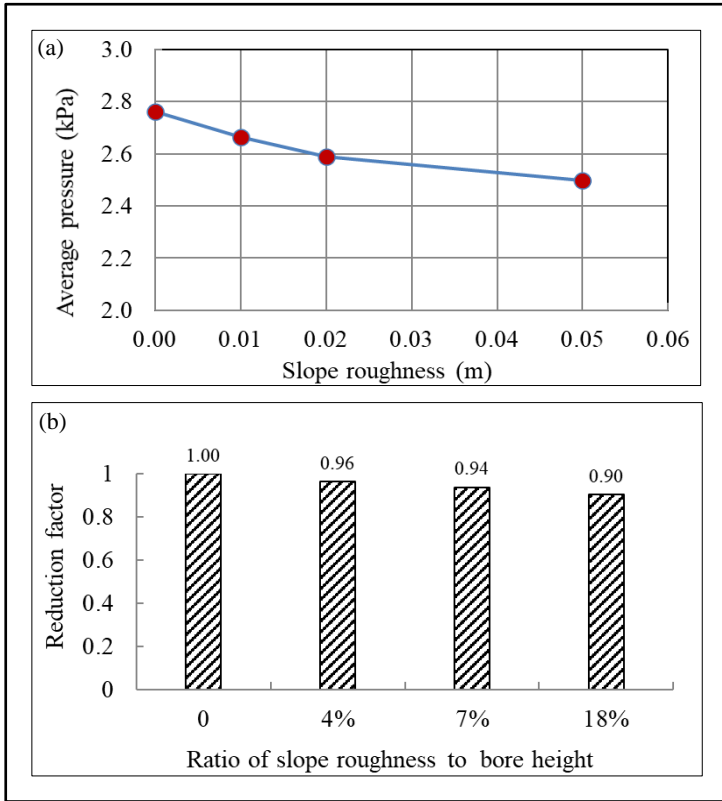


Figure 10. Sensitivity of the tsunami pressure to the surface roughness of wharf deck

4. Conclusion and Recommendation

The results showed that the numerical model was more suitable for predicting the uplift pressure with small wharf slope angles. The numerical results revealed the same four stages as the experimental evidence: the tsunami bore generation, stabilization, propagation and impact stages. The progress of the tsunami bore impacting on the wharf had four stages, namely front-climbing, front-hitting, water accumulation and quasi-steady stages. The water levels, velocity fields and pressure contours varied significantly between the different impact stages. The average tsunami pressures exerted on the deck were influenced by the wharf configurations. Average pressure was constant for deck lengths smaller than the deck height, and decreased with increasing deck

length for deck lengths larger than the deck height. The reduction factor of the tsunami pressure decreased with increasing gap length for gap lengths up to 50% of the deck length. The reduction factor of the tsunami pressure decreased with increasing surface roughness for surface roughness up to 18% of the bore height. Although this study provided insight into tsunami-wharf interaction, large-scale physical model studies will be needed to scrutinize the roles of deck length, gap length and roughness of deck materials against tsunami pressure in the future.

5. Acknowledgement

This work was supported by the National Natural Science Foundation of China (Grant No. 51809047), the Natural Science Foundation of Fujian Province, China (Grant No. 2019J05029) and the Natural Hazards Research Platform, New Zealand (2012-GNS-03-NHRP). Also, the valuable suggestions from Graham Macky and Hamed Benisi are appreciated.

6. References

- Biscarini, C., Di Francesco, S., & Manciola, P. (2010). CFD modelling approach for dam break flow studies. *Hydrology and Earth System Sciences*, 14, 705-718. <https://doi.org/10.5194/hess-14-705-2010>
- City and County of Honolulu (CCH). (2000). Building code (chapter 16, article 11). Honolulu, Hawaii: Department of Planning and Permitting.
- Chao, A., & Liu, P.L.F. (2014). Characteristics of leading tsunami waves generated in three recent tsunami events. *Journal of Earthquake and Tsunami*, 8(3), 1440001. <https://doi.org/10.1142/S1793431114400016>
- Chanson, H. (2006). Tsunami surges on dry coastal plains: Application of dam break wave equations. *Coastal Engineering Journal*, 48(4), 355-370. <https://doi.org/10.1142/S0578563406001477>
- Chen, C., Melville, B.W., & Nandasena, N.A.K. (2018). An experimental investigation of tsunami bore impacts on a coastal bridge model with different contraction ratios. *Journal of Coastal Research*, 34(2), 460-469.
- Chen, C., Melville, B.W., & Nandasena, N.A.K. (2016). Experimental study of uplift loads due to tsunami bore impact on a wharf model. *Coastal Engineering*, 117, 126-137. <https://doi.org/10.1016/j.coastaleng.2016.08.001>

Cheng, D., Zhao, X., Zhang, D., & Chen, Y. (2017). Numerical study of dam-break induced tsunami-like bore with a hump of different slopes. *China Ocean Engineering*, 31(6), 683-692. <https://doi.org/10.1007/s13344-017-0078-2>

Crespo, A.J., Gómez-Gesteira, M., & Dalrymple, R.A. (2008). Modeling dam break behavior over a wet bed by a SPH technique. *Journal of Waterway, Port, Coastal, and Ocean Engineering*, 134(6), 313-320. [https://doi.org/10.1061/\(ASCE\)0733-950X\(2008\)134:6\(313\)](https://doi.org/10.1061/(ASCE)0733-950X(2008)134:6(313))

Deng, X., Liu, H., & Jiang, Z. (2016). Swash flow properties with bottom resistance based on the method of characteristics. *Coastal Engineering*, 114, 25-34. <https://doi.org/10.1016/j.coastaleng.2016.03.012>

Dressler, R.F. (1952). Hydraulic resistance effect upon the dam-break functions. *Journal of Research of the National Bureau of Standards*, 49(3), 217-225.

Flow Science, Inc. (2012). *Flow-3D user's manuals*. Santa Fe, NM: Flow Science, Inc.

Federal Emergency Management Agency (FEMA). (2012). *Guidelines for design of structures for vertical evacuation from tsunamis (FEMA P646)*. Washington, USA: Federal Emergency Management Agency.

Kihara, N., Niida, Y., Takabatake, D., Kaida, H., Shibayama, A., & Miyagawa, Y. (2015). Large-scale experiments on tsunami-induced pressure on a vertical tide wall. *Coastal Engineering*, 99, 46-63. <https://doi.org/10.1016/j.coastaleng.2015.02.009>

Ko, H.T.S., & Yeh, H. (2018). On the splash-up of tsunami bore impact. *Coastal Engineering*, 131, 1-11. <https://doi.org/10.1016/j.coastaleng.2017.10.002>

Lauber, G., & Hager, W.H. (1998). Experiments to dambreak wave: Horizontal channel. *Journal of Hydraulic Research*, 36(3), 291-307. <https://doi.org/10.1080/00221689809498620>

Liu, H., Liu, H., & Guo, L. (2017). Experimental study on the dam-break hydrographs at the gate location. *Journal of Ocean University of China*, 16(4), 697-702. <https://doi.org/10.1007/s11802-017-3470-x>

Marsooli, R., & Wu, W. (2014). 3-D finite-volume model of dam-break flow over uneven beds based on VOF method. *Advances in Water Resources*, 70, 104-117. <https://doi.org/10.1016/j.advwatres.2014.04.020>

Nandasena, N.A.K., & Tanaka, N. (2013). Boulder transport by high energy: Numerical model-fitting experimental observations. *Ocean Engineering*, 57, 163-179. <https://doi.org/10.1016/j.oceaneng.2012.09.012>

Nouri, Y., Nistor, I., Palermo, D., & Cornett, A. (2010). Experimental investigation of tsunami impact on free standing structures. *Coastal Engineering Journal*, 52(1), 43-70.

Rahman, S., Akib, S., & Khan, M.T.R. (2014). Experimental study on tsunami risk reduction on coastal building fronted by sea wall. *The Scientific World Journal*, 729357. <https://doi.org/10.1155/2014/729357>

Shafiei, S., Melville, B.W., & Shamseldin, A.Y. (2016). Experimental investigation of tsunami bore impact force and pressure on a square prism. *Coastal Engineering*, 110, 1-16. <https://doi.org/10.1016/j.coastaleng.2015.12.006>

Shafiei, S., Melville, B.W., & Shamseldin, A.Y. (2018). Instant tsunami bore pressure and force on a cylindrical structure. *Journal of Hydro-environment Research*, 19, 28-40. <https://doi.org/10.1016/j.jher.2018.01.004>

Wei, Z., Dalrymple, R.A., & Rustico, E. (2016). Simulation of nearshore tsunami breaking by smoothed particle hydrodynamics method. *Journal of Waterway, Port, Coastal, and Ocean Engineering*, 142(4), 05016001. [https://doi.org/10.1061/\(ASCE\)W.1943-5460.0000334](https://doi.org/10.1061/(ASCE)W.1943-5460.0000334)

Ye, Z., & Zhao, X. (2017). Investigation of water-water interface in dam break flow with a wet bed. *Journal of Hydrology*, 548, 104-120. <https://doi.org/10.1016/j.jhydro.2017.02.055>

Zheng, X., Ma, Q., & Duan, W. (2014). Comparative study of different SPH schemes on simulating violent water wave impact flows. *China Ocean Engineering*, 28(6), 791-806. <https://doi.org/10.1007/s13344-014-0061-0>